Biochemical Pharmacology 158 (2018) 286–297

Contents lists available at ScienceDirect

Biochemical Pharmacology

journal homepage: www.elsevier.com/locate/biochempharm

Identification of a 2-propanol analogue modulating the non-enzymatic function of indoleamine 2,3-dioxygenase 1

E. Albini[a], A. Coletti[b], F. Greco[b], M.T. Pallotta[a], G. Mondanelli[a], M. Gargaro[a], M.L. Belladonna[a], C. Volpi[a], R. Bianchi[a], U. Grohmann[a], A. Macchiarulo[b,1], C. Orabona[a,*,1]

[a] Department of Experimental Medicine, University of Perugia, P.le Gambuli, 06132 Perugia, Italy
[b] Department of Pharmaceutical Sciences, University of Perugia, via del Liceo 1, 06123 Perugia, Italy

ARTICLE INFO

Keywords:
IDO1
Kynurenine
Immunoreceptor Tyrosine-based Inhibitory Motifs (ITIM)
Fragment-based screening
Thermophoresis

ABSTRACT

Indoleamine 2,3 dioxygenase 1 (IDO1) is a metabolic enzyme that catalyzes the conversion of the essential amino acid tryptophan (Trp) into a series of immunoactive catabolites, collectively known as kynurenines. Through the depletion of Trp and the generation of kynurenines, IDO1 represents a key regulator of the immune responses involved in physiologic homeostasis as well as in neoplastic and autoimmune pathologies. The IDO1 enzyme has been described as an important immune checkpoint to be targeted by catalytic inhibitors in the treatment of cancer. In contrast, a defective expression/activity of the enzyme has been demonstrated in autoimmune diseases. Beside its catalytic activity, the IDO1 protein is endowed with an additional function associated with the presence of two immunoreceptor tyrosine-based inhibitory motifs (ITIMs), which, once phosphorylated, bind SHP phosphatases and mediate a long-term immunoregulatory activity of IDO1. Herein, we report the screening of a focused library of molecules bearing a propanol core by a protocol combining microscale thermophoresis (MST) analysis and a cellular assay. As a result, the combined screening identified a 2-propanolol analogue, VIS351, as the first potent activator of the ITIM-mediated function of the IDO1 enzyme. VIS351 displayed a good dissociation constant (Kd = 1.90 μM) for IDO1 and a moderate cellular inhibitor activity (IC_{50} = 11.463 μM), although it did not show any catalytic inhibition of the recombinant IDO1 enzyme. Because we previously demonstrated that the enzymatic and non-enzymatic (i.e., ITIM-mediated) functions of IDO1 reside in different conformations of the protein, we hypothesized that in the cellular system VIS351 may shift the dynamic conformational balance towards the ITIM-favoring folding of IDO1, resulting in the activation of the signaling rather than catalytic activity of IDO1. We demonstrated that VIS351 activated the ITIM-mediated signaling of IDO1 also in mouse plasmacytoid dendritic cells, conferring those cells an immunosuppressive phenotype detectable *in vivo*. Thus the manuscript describes for the first time a small molecule as a positive modulator of IDO1 signaling function, paving the basis for an innovative approach to develop first-in-class drugs acting on the IDO1 target.

1. Introduction

Indoleamine 2,3 dioxygenase 1 (IDO1) is a metabolic enzyme that catalyzes the conversion of the essential amino acid L-tryptophan (Trp) into a series of immunoactive catabolites, collectively known as kynurenines. The IDO1 enzyme has been largely described as a powerful regulator of the immune responses, since IDO1, through the depletion of Trp and the generation of bioactive metabolites can create an extracellular milieu that promotes immune tolerance. IDO1 activity has been demonstrated to inhibit effector T cells, favor regulatory T cell differentiation and program dendritic cells (DCs) and macrophages toward an immunosuppressive phenotype [1–3]. The IDO1 enzyme plays a physiological role in guaranteeing several immune privileged sites. Human studies indicated a constitutive IDO1 expression in the placenta, eye, and pancreas [4–6]. Moreover, IDO1 is involved in the pathogenesis and severity of different disease conditions, including chronic inflammation, infectious disease, allergic and autoimmune disorders, transplantation, neuropathology, and cancer [7–11]. The enzyme has been recognized as an important immune checkpoint for the development of catalytic inhibitors in oncology [12]. In contrast, a

* Corresponding author.
E-mail address: ciriana.orabona@unipg.it (C. Orabona).
[1] These authors shared senior authorship.

https://doi.org/10.1016/j.bcp.2018.10.033
Received 11 September 2018; Accepted 30 October 2018
Available online 01 November 2018

defective expression/activity of the enzyme has been described in autoimmune diseases [13–15] and thus drugs capable of enhancing IDO1 immunoregulatory mechanisms are demanding.

IDO1 exerts its immunoregulatory effects via several molecular mechanisms, including the deprivation of Trp and its conversion into L-kynurenine (Kyn), a ligand of the aryl hydrocarbon receptor (AhR) [16,17] and the following conversion into down-stream bioactive Trp catabolites [1,18,19]. Moreover, IDO1 is endowed with non-enzymatic activity that involves tyrosine phosphorylation of the immunoreceptor tyrosine-based inhibitory motifs (ITIM) 1 and 2 present in its non-catalytic, small domain. Phosphorylated IDO1 ITIMs generate in IDO1 two docking sites for Src homology 2 (SH2)-containing proteins, such as the suppressor of cytokine signaling (SOCS)3 and tyrosine phosphatases SHP-1 and SHP-2. The association with either partners (i.e., SOCS3 or SHP phosphatases) can modulate the enzyme half-life toward an opposite fate. In an IL-6-driven inflammatory context, SOCS3 becomes highly expressed in dendritic cells (DCs) and shortens IDO1 half-life by accelerating its proteasomal degradation. By contrast, the association of SHP phosphatases to IDO1 prolongs the enzyme half-life through the activation of a feedforward loop that sustains the *de novo* synthesis of the enzyme and TGF-β, a required condition for restraining autoimmunity and chronic diseases [20–22]. IDO1 mutants, mimicking the stable phosphorylation of ITIMs, show a complete loss of catalytic activity, a result that might be traced to a major change in protein folding. Despite the loss of catalytic activity, IDO1 mutants maintain their ability to trigger ITIM-related functions [23]. Thus the enzymatic and non-enzymatic functions of IDO1 may reside in different conformations of the protein and could be mutually exclusive, suggesting a dynamic balance between the catalytically active and the ITIM-favoring conformations of IDO1, occurring in cells. In the current manuscript, we describe a screening approach that led us to identify for the first time a positive modulator of the ITIM-function — rather than the catalytic activity — of the IDO1 protein.

2. Materials and methods

2.1. Animals and reagents

Female wild-type C57BL/6 mice of 6-wks of age were purchased from Charles River Breeding Laboratories Italia (Milan, Italy) and female IDO1-deficient (*Ido1*$^{-/-}$) C57BL/6 mice were from Jackson Laboratories (ME, USA) and bred at Charles River Breeding Laboratories. All animals were housed and fed under specific pathogen-free conditions in the animal facility of the University of Perugia. All *in vivo* studies were in compliance with National (Italian Animal Welfare Assurance A-3143-01) and Perugia University Animal Care and Use Committee guidelines. Cycloheximide and DMSO were purchased from Sigma-Aldrich (MO, USA). The *H-2*D^{b}-restricted HY peptide (WMHH-NMDLI) — containing the immunodominant epitope of male mouse-specific minor transplantation antigen — was synthesized by BioFab Research (Rome, Italy). Recombinant human IDO1 (rhIDO1) (residues 1-403) was purchased from Giotto Biotech S.r.l. (Firenze, Italy). All tested compounds were purchased from Life Chemicals Europe (Munich, Germany). The NLG919 analogue was purchased from Selleckchem (Huston, TX, USA).

2.2. Microscale thermophoresis (MST)

MST experiments were carried out using the Monolith NT.115 instrument (NanoTemper Techonologies, Munich, Germany). The assay is based on the use of 16 capillary tubes that are filled with a fluorescent dye-labeled target protein and a serial titration of unlabeled ligand. Capillary tubes are then illuminated with an infrared laser that generates a temperature gradient. The protein/ligand complex migrates along this gradient causing changes in the observed fluorescence. These signals are used to generate a binding curve as a function of ligand concentration that is then analyzed to assess the K_d value [24]. As previously reported [25], fluorescence labeling of rhIDO1 was performed following the manufacturer's instructions for N-hydroxysuccinimide (NHS) coupling of the dye NT647 to lysine residues. The stability of NT647-rhIDO1 and unlabeled rhIDO1 protein in the experimental conditions was checked using circular dichroism, as previously reported [25]. Binding experiments were carried out using premium-coated capillaries and MST buffer containing 2% DMSO and 2 mM DTT. Compound stocks (50 mM) in DMSO were diluted in the assay buffer to reach the highest soluble concentration (1 mM). In MST experiments, 16-fold 1:1 serial dilutions of each compound were mixed with NT647-rhIDO1 (45 nM) in a final reaction volume of 20 µl. After 10 min of incubation at RT, mix were loaded into 16 premium-coated capillary tubes and inserted in the chip tray of Monolith NT.115 for thermophoresis analysis and the appraisal of K_d values. Signals were recorded at 40% MST and 20% LED power. K_d values were calculated from compound concentration-dependent changes in normalized fluorescence (Fnorm) of NT647-rhIDO1 after 21 s of thermophoresis. Each compound was tested in triplicate and data analyzed using *MO Affinity Analysis* software (NanoTemper Technologies, Munich, Germany). Confidence values (±) were indicated next to K_d value for each of tested compound. The binding efficiency index (BEI) was calculated for each compound (BEI = pK_d/MW) [26].

2.3. Docking studies

The crystal structure of IDO1 in complex with the NLG919 analogue (PDB code: 5EK3, resolution = 2.20 Å) [27] was downloaded from the Protein Data Bank [28], and its chain A was prepared by adding hydrogen atoms with relative ionization states at pH 7.0, using the Protein Preparation Wizard implemented in Maestro v10.1 (Maestro, version 10.1, Schrödinger, LLC, New York, NY, 2015). The unsolved loop 361–379 was reconstructed with Prime v3.9 (Prime, version 3.9, Schrödinger, LLC, New York, NY, 2015), while the formal charge of the iron was set as FeIII. The molecular structure of VIS351 was refined with LigPrep v3.3, generating all ionization and tautomer states at pH 7 ± 2. Docking studies were carried out using Glide v6.6 with the default extra-precision (XP) method combined with an expanded sampling mode (Glide, version 6.6, Schrödinger, LLC, New York, NY, 2015). The number of poses to keep for the initial phase of docking was set to 50.000 in a scoring window of 500 kcal/mol. The energy minimization for the best 800 poses was carried out performing 10.000 maximum number of steps. The docking grid was defined with the centre located on the center of mass of the co-crystallized ligand in 5EK3, and the inner grid box sized at 10 × 10 × 10 Å.

2.4. Cellular assays

Cells of P1.HTR, a highly transfectable clonal variant of mouse mastocytoma P815 [29], were transfected by electroporation with plasmid constructs coding for mouse IDO1 (P1.IDO1) or tryptophan 2,3-dioxygenase (P1.TDO). Stable transfectant cell lines were obtained by puromycin selection. Both cell lines were cultured in Iscove's Modified Dulbecco's Medium (Gibco, Invitrogen CA, USA) supplemented with 10% FCS (Gibco, Invitrogen CA, USA), 1 mM glutamine (Gibco, Invitrogen CA, USA) and penicillin/streptomycin (Gibco, Invitrogen CA, USA) at 37 °C in a humidified 7% CO_2 incubator. In every cellular assay, cell lines were used at a passage number not exceeding the 10th. For evaluating the inhibition of mouse IDO1 in a cellular context, 1×10^5 P1.IDO1 cells were incubated in a final volume of 400 µl with 30 µM of compound (single point concentration) for 16 h in a 48-well plate. The control was represented by cells incubated with an equivalent volume of DMSO, the vehicle in which compounds have been solubilized. After the incubation, supernatants of cell cultures were recovered and Kyn concentration was detected by HPLC. Results are represented as the percentage of inhibition of Kyn production as

compared to cells incubated with vehicle alone. Dose-response curves for extrapolating the cellular IC_{50} were built through the same cellular assay, by incubating P1.IDO1 cells with 3-fold serial dilutions of either the NLG919 analogue or VIS351. For estimating the cell specificity of the inhibitory effect, both P1.IDO1 and P1.TDO cell lines were incubated in the same experimental condition described above and incubated with three different 10-fold dilutions of VIS351. Every cell assay was conducted in triplicate and repeated three times. Results are represented as the mean ± standard deviation of the Kyn fold change (Kyn FC), i.e., the ratio between Kyn concentration secreted in the supernatant of the compound-treated and DMSO-treated cells. In plasmacytoid dendritic cells (pDCs), culture supernatants were collected and used for Kyn analysis after incubation overnight of the cells with VIS351 at 30 μM or DMSO, as control.

2.5. LDH cytotoxicity assay

Molecule-dependent cytotoxicity was estimated using the LDH-Cytotoxicity Assay Kit (Abcam, Cambridge, UK), according to the manufacturer's instructions. 1×10^4 P1.IDO1 cells were plated in a flat-bottomed 96-well plate containing a final volume of 200 μl of medium and 2-fold dilutions in the range of 1.25–80.00 μM concentration of the molecules. P1.IDO1 cells incubated with DMSO alone, the vehicle used to dilute the molecules, served as spontaneous LDH activity controls. For the maximum LDH activity control, P1.IDO1 cells were incubated with medium containing 1% TritonX-100 (Sigma-Aldrich, MO, USA). In all conditions, cells were incubated in triplicate at 37 °C, 7% CO_2. After 16 h, an aliquot (100 μl) of each sample was transferred into a new 96-well plate, mixed with 100 μl of Reaction Mixture and incubated for 30 min at RT in the dark. Absorbance values at 490 nm and 620 nm were measured using a Tecan Infinite M200 reader (Mannedorf, Switzerland). The LDH activity was calculated by subtracting the 620 nm absorbance value (due to plate absorbance) from the 490 nm absorbance. Cell viability percentage was shown as the reciprocal of the amount of LDH released by the cell sample.

2.6. Enzymatic assay

IDO1 enzymatic assay was carried out according to the protocol described previously [30]. In brief, compounds or DMSO, as control, were mixed in a final volume of 200 μl of a standard reaction mixture containing 50 mM potassium phosphate buffer (pH 6.5), 20 mM ascorbic acid (neutralized with NaOH), 200 μg/mL catalase, 10 μM methylene blue, 20 μM Trp (Sigma-Aldrich, MO, USA) and 0.125 μg rhIDO1 protein (Giotto Biotech S.r.l., Firenze). To estimate enzymatic IC_{50}, VIS351 and NLG919 (as reference inhibitor) were seven times 10-fold diluted, starting from the highest soluble concentration (2 mM). The reaction was carried out at 37 °C for 60 min and stopped by the addition of 40 μl $HClO_4$ (Sigma-Aldrich, MO, USA). To complete the hydrolysis of N-formyl-kynurenine into Kyn, samples were heated at 65 °C for 15 min and then centrifuged at 12.000 rpm for 7 min at RT. The supernatant (200 μl) was transferred into a new Eppendorf tube and used for Kyn analysis. Each enzymatic assay was conducted in triplicate and repeated three times. Results are represented as the mean ± standard deviation of the Kyn FC, i.e., the ratio between Kyn concentration in samples with compounds and control (i.e., DMSO alone).

2.7. IDO1 protein degradation analysis

P1.IDO1 cells (2×10^5) were pre-treated with 10 μg/ml of the protein synthesis inhibitor cycloheximide in a final volume of 400 μl for 30 min at 37 °C. Then, cells were stimulated with VIS351 (30 μM) or DMSO as control, for 0, 1, 3 and 6 h and immediately lysed for IDO1 protein expression analysis by immunoblotting. Protein lysates were subjected to SDS-PAGE and electro-blotted onto 0.2 μm nitrocellulose membranes (Bio-Rad, CA, USA). Membranes were blocked with 5% non-fat dried milk in TBS and probed with a rabbit polyclonal antibody specific for mouse IDO1, raised in our laboratory [23] in combination with an appropriate horseradish peroxidase-conjugated antibody (Millipore, MA, USA), followed by enhanced chemiluminescence (ECL) (Bio-Rad, CA, USA). Anti-β-tubulin (Sigma-Aldrich, MO, USA) was used as a normalizer. In each experiment, the densitometric analysis of specific signals was performed by ChemiDoc XRS + Imagin System (Bio-Rad, CA, USA), within a linear range of blot exposure, selecting the two lowest exposure times required for detecting signals. Results of the densitometric analysis were represented as the mean ± SD of three different Western blot analyses. For each sample, the ratio of normalized IDO1 protein at each time point over the time 0 was shown.

2.8. Kynurenine and cytokines measurements

Detection of Kyn concentrations was performed by using a Perkin Elmer, series 200 HPLC instrument (MA, USA). A Kinetex® C18 column (250 × 4.6 mm, 5 μm, 100 Å; Phenomenex, USA), maintained at the temperature of 25 °C and pressure of 1800 PSI, was used. A sample volume of 300 μl was injected and eluted by a mobile phase containing 10 mM NaH_2PO_4 pH 3.0 (99%) and methanol (1%) (Sigma-Aldrich, MO, USA), with a flow rate of 1 ml/min. Kyn was detected at 360 nm by an UV detector. The software TURBOCHROM 4 was used for evaluating the concentration of Kyn in samples by mean of a calibration curve. The detection limit of the analysis was 0.05 μM. Mouse TGF-β (Affymetrix, Santa Clara, CA, USA), IL-6 (eBioscience – Termo Fisher Scientific, MS, USA) and IL-10 (Life Technologies, CA, USA) levels were measured in culture supernatants by specific kit ELISA, according to the manufacturer's recommendations.

2.9. Phosphatase assay

P1.IDO1 cells were pre-incubated for 4 h with VIS351 (30 μM) or DMSO as control, before assessing the phosphatase activity associated with the IDO1 protein. For each condition, the IDO1 protein was immunoprecipitated from 6×10^6 cells lysed in 400 μl of Lysis Buffer (50 mM Tris-HCl pH 7.5, 150 mM NaCl, 1% Nonidet P-40 and a cocktail of protease inhibitors). The IDO1 protein was immunoprecipitated overnight at 4 °C by a specific polyclonal rabbit antibody raised in our lab, followed by addition of Protein G-Sepharose (Sigma-Aldrich, MO, USA) for 2 h. The phosphatase activity associated with immunoprecipitated IDO1 was assessed by a specific kit purchased from Promega (WI, USA), according to the manufacturer's instructions.

2.10. DC purification and skin test assay

All purification procedures of splenic wild-type (WT) or *Ido1*$^{-/-}$ pDCs and $CD8^-$ DCs (hereafter referred to as cDCs, for conventional DCs) were conducted as previously described in [21,31]. A skin test assay was used for measurements of major histocompatibility complex class I-restricted delayed-type hypersensitivity (DTH) responses to the HY peptide in C57BL/6 female recipient mice [21,32]. For *in vivo* immunization, 3×10^5 peptide-loaded cDCs, combined with a minority fraction (5%) of peptide-loaded WT or *Ido1*$^{-/-}$ pDCs, were injected subcutaneously into recipient mice. After two weeks, mice were challenged intrafootpad with the HY peptide in the absence of DCs (experimental footpad) or with vehicle alone (control counterpart). Twenty-four hours later, mice were sacrificed, footpads were removed and the change in the weight of the peptide-injected footpad over that of the vehicle-injected counterpart (i.e., internal control) was measured. A significant increase in mean weight of the experimental over the control footpads will then demonstrate and quantify any delayed-type, antigen-specific hypersensitivity response. Results are represented as the mean weight ± SD of the experimental footpads over that of control, vehicle-injected counterparts. The significance marked on each

condition is referred to a two-tailed paired *t* test (experimental vs control footpads) for each group of mice ($n = 6$).

2.11. Flow cytometry

Two weeks after the vaccination of mice, the frequencies of IFN-γ-producing $CD3^+$ $CD44^+$ T cells, $Foxp3^+$ $CD4^+$ T cells expressing the latency associated peptide (LAP; the surface form of TGF-β), and IL-10-producing T cells were determined by intracellular staining in popliteal lymph nodes (pLN) of peptide antigen-challenged footpads. Freshly isolated pLN cells were incubated with PMA (50 ng/ml; Sigma-Aldrich, MO, USA), ionomycin (0.8 μg/ml, Sigma-Aldrich, MO, USA), brefeldin A (3 μg/ml; eBioscience, CA, USA) for 4 h at 37 °C, 7% CO_2. Phenotypic characterization of $CD8^+$ and $CD4^+$ T cell subsets was performed by extracellular staining using the following Abs: Fc block (2.4G2; BD Biosciences, CA, USA), APC-CD3 (145-2C11; Biolegend, CA, USA), PE-DazzleTM-B220 (RA3-6B2; Biolegend, CA, USA), BV510-CD4 (RM4-5; BD Horizon, CA, USA), PerCP-Cy5.5-CD8 (53.6.7; BD Pharmingen, CA, USA), BV786-CD44 (IM7; BD Horizon, CA, USA), BV421-LAP (TW716B4; BD Horizon, CA, USA). For intracellular staining, the following antibodies were used: Alexa Fluor 488-IFN-γ (XMG1.2; eBioscience, CA, USA), BV711-IL10 (JES5-16E3; BD Horizon CA, USA), PE-Foxp3 (FJK-16 s; eBioscience, CA, USA). Samples were analysed on LSR Fortessa (BD Biosciences, CA, USA) flow cytometer, using FlowJo analysis software (Tree Star, OR, USA).

2.12. Real-time PCR analysis

Expression of *Ido1, Tgfb1, Ptpn6, Ptpn11* and *Socs3* genes was analyzed by Real-Time PCR, as described [21] using the specific primers reported in Table 1. Real time PCR assays were performed using Stratagene Mx3005P (Agilent Technologies, CA, USA). The cycling program consisted of a pre-incubation of 10 min at 95 °C followed by 40 cycles consisting of 10 s at 95 °C, 30 s at 60 °C and 1 s at 72 °C. mRNA levels were normalized to the expression of the *Gapdh* housekeeping gene. The Ct number was measured using the MxPro-Mx3005P software (Agilent Technologies, CA, USA). Values were expressed as the ratio of *Gapdh*-normalized transcript expression of VIS351 treated-pDCs to *Gapdh*-normalized transcript expression of untreated pDCs.

3. Results

3.1. Analogue-based screening

We previously reported a fragment-based screening campaign to identify building blocks as starting points for the development of IDO1 inhibitors. As a result, we disclosed 14 fragments binding IDO1 with different dissociation constants, and belonging to different chemical classes [25]. In particular, one active fragment bearing a propanol scaffold (**1**) was found as structurally similar to the NLG919 analogue (**2**) (Fig. 1). Remarkably, this fragment was devoid of a chemical group able to coordinate the iron atom of the heme cofactor, as represented in the crystal structure of **2** in complex with IDO1 (Fig. 2). Very few IDO1 inhibitors binding the enzyme without a direct interaction with the iron heme have been reported in literature [25]. The most advanced compounds of this kind include D-1-methyl-tryptophan (**3**) and PF-06840003 (**4**) (Fig. 1), which are in clinical trials as single agent therapy (e.g., NCT00567931 and NCT02764151) or in combination therapy with cytotoxic agents, vaccines or checkpoint inhibitors (e.g., NCT01191216, NCT01042535 and NCT02073123). Recently, Nelp et al. described a promising class of compounds that target the apo-form of IDO1 and inhibit the enzyme in a specific and effective manner [33].

With the aim of further exploring functional activities of this class of compounds, we firstly embarked on a hit-to-lead optimization strategy, expanding the series of IDO1 ligands endowed with a central propanol scaffold. Accordingly, analogue-based searches around compound **1** ($K_d = 96.7$ μM) were carried out using commercial compound libraries and a total of 20 molecules (**5–24**) (Fig. 3) bearing a propanol core was purchased and used for MST binding experiments against IDO1. Based on the results reported in Table 2, inspection of dissociation constants (K_d) values revealed that four compounds (**13, 14, 21, 22**) bind IDO1 with a K_d in the low micromolar range (i.e., < 10 μM). In particular, a comparative analysis of the binding efficiency index (BEI) suggested compound **14** as identical to the NLG919 analogue (**2**) in terms of efficiency of ligand/protein interaction [26], despite the former lacks any hydrogen bond and/or coordinative interaction to the heme group.

Table 1
Primer sequences used in the study.

Gene	Primer sequence	
Ido1	F	5′-CGATGTTCGAAAGGTGCTGC-3′
	R	5′-GCAGGAGAAGCTGCGATTTC-3′
Tgfb1	F	5′-CACAGAGAAGAACTGCTGTG-3′
	R	5′-AGGAGCGCACAATCATGTTG-3′
Ptpn6	F	5′-CAGCTGCTAGGTCCAGATGAGA-3′
	R	5′-CAGCTCAGGTACTGGTAGTGC-3′
Ptpn11	F	5′-GAGCTGAAATACGACGTTGGTGG-3′
	R	5′-TGCATTCCTGTTGCTGGAGCGT-3′
Socs3	F	5′-CAG CCT GCG CCT CAA GAC CTT-3′
	R	5′-GCA CCA GCT TGA GTA CAC AGT CG-3′
Gapdh	F	5′-CTGCCCAGAACATCATCCCT-3′
	R	5′-ACT TGG CAG GTT TCT CCA GG-3′

Abbreviations: F, forward; R, reverse.

3.2. Combining MST to cellular screening

In order to achieve early information on the efficacy of the 20 molecules (5–24) in a cellular system, the MST approach was combined with a cellular assay for selecting those molecules featured by a good dissociation constant ($K_d < 10$ μM) and the ability to permeate the cell. Specifically, the 20 compounds (**5–24**), previously evaluated in MST experiments, were also tested for their ability to inhibit the conversion of Trp into Kyn in the mastocytoma cell line P1.IDO1, stably expressing the mouse protein IDO1 (mIDO1), as described [25]. The reference molecule used in the cellular screening was represented by the NLG919 analogue (**2**). Previous published data demonstrated an excellent correlation between results obtained from mIDO1 expressed by a cell system and the human IDO1 (hIDO1) in cell-free assays [34,35], since mouse and human sequences of IDO1 share a 61% of identity and, most importantly, both catalytic domain and the ITIM sequences of human and mouse proteins are highly conserved [22,36]. Each compound, included the reference molecule NLG919, was tested in the cellular assay at the single concentration of 30 μM for 16 h and Kyn secretion in cell culture supernatants was detected by HPLC analysis.

As expected, NLG919 abrogated Kyn production with a nearly 90% of inhibition. The majority of compounds that had shown a $K_d > 10$ μM revealed an inhibitory activity below 50%. In spite of their high K_d value, molecules **10** and **16** (respectively, $K_d > 1{,}000$ μM and $K_d = 59.5$ μM) resulted in an inhibitory activity of nearly 65%. Among the four compounds (**13, 14, 21, 22**) with a $K_d < 10$ μM, only molecules **14** and **21** demonstrated an inhibitory activity above 50%, while molecules **13** and **22** showed an inhibitory activity below 40% (Fig. 4A).

Based on the usefulness of a combined screening coming from both a cell-free (i.e., MST) and a cellular assay, we computed a combined screening (CS) score for each compound as the ratio between the inhibitory activity (%) in the cell assay and the K_d value observed in MST. As a result, a higher inhibitory activity combined with a lower K_d value will result in a high CS score. Estimation of the CS score confirmed

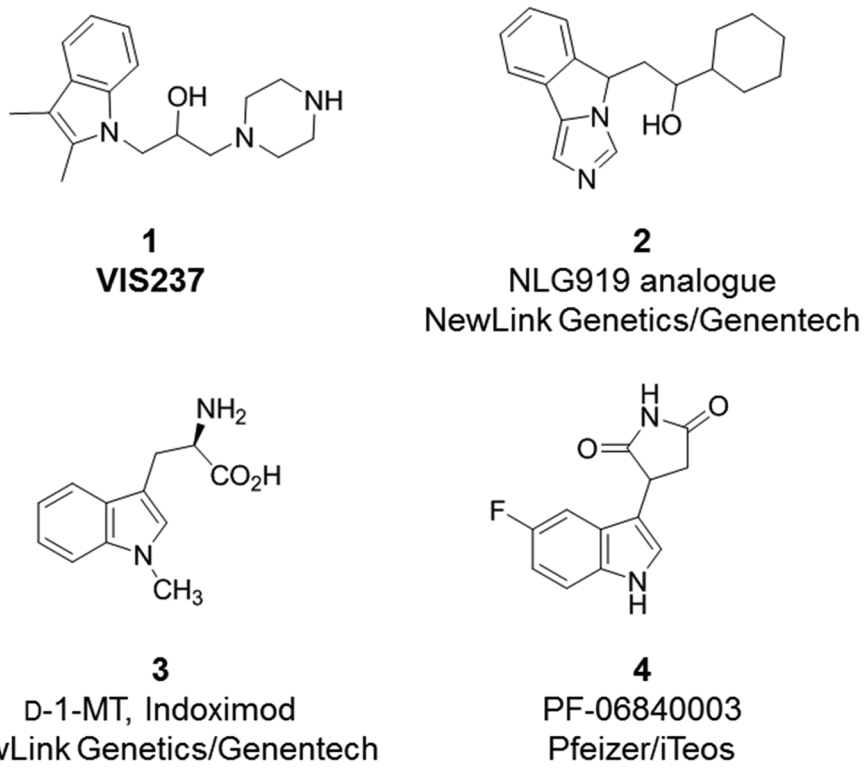

Fig. 1. Chemical structures of the original propanol scaffold VIS237 (**1**), NLG919 analogue (**2**), D-1-MT (**3**) and PF-06840003 (**4**).

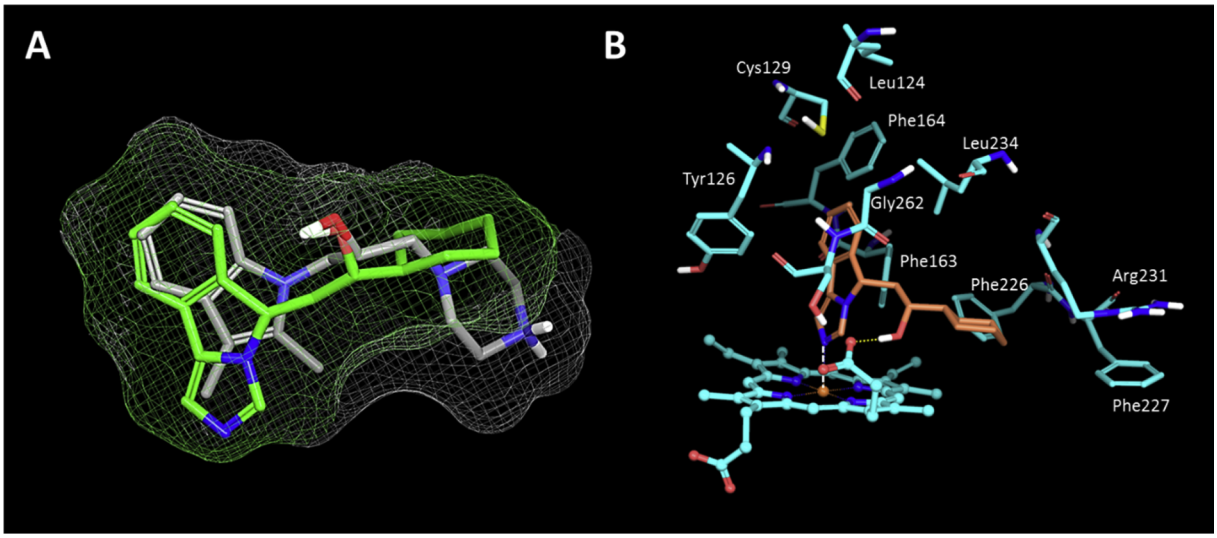

Fig. 2. A) Structural and shape similarities between VIS237 (**1**, grey coloured carbon) and the NLG919 analogue (**2**, green coloured carbons); B) Binding mode of the NLG919 analogue to IDO1 according to the crystal complex (pdb code: 5EK3). (For interpretation of the references to colour in this figure legend, the reader is referred to the web version of this article.)

compounds **14** and **21** as those molecules having the highest score among the analyzed analogues, even much higher than that of the reference compound NLG919 (Fig. 4B). In contrast, molecules **13** and **22** (K_d = 6.3 μM and K_d = 4.0 μM, respectively), resulted in a very low CS score that led us to discard them from further analysis. Overall, the above combined screening corroborated the validity of the method and allowed us to select the compounds **14** and **21**, both characterized by a good K_d and efficacy in the cell system expressing the target protein.

3.3. Cellular and enzymatic IC_{50} determination

In order to exclude false positives due to a cytotoxic effect of the molecules, we firstly analyzed molecules **14** and **21** to exclude that the decreased Kyn levels secreted after cell incubation could be caused by a cytotoxic effect. To this purpose, we used the LDH-cytotoxicity assay that measures the activity of the LDH enzyme released from damaged cells. By using seven 2-fold dilutions in the 1.25–80.00 μM concentration range, we observed a cytotoxic effect for the compound **21** starting from 5 μM that decreased the cell viability to 50%. In contrast, compound **14** showed a good safety at all tested concentrations (Fig. 5A). These data suggested that the inhibition of Kyn production by compound **21,** observed along cellular screenings, was probably due to a decreased cellular viability rather than a specific inhibition of the catalytic activity of IDO1. For this reason, our study focused on molecule

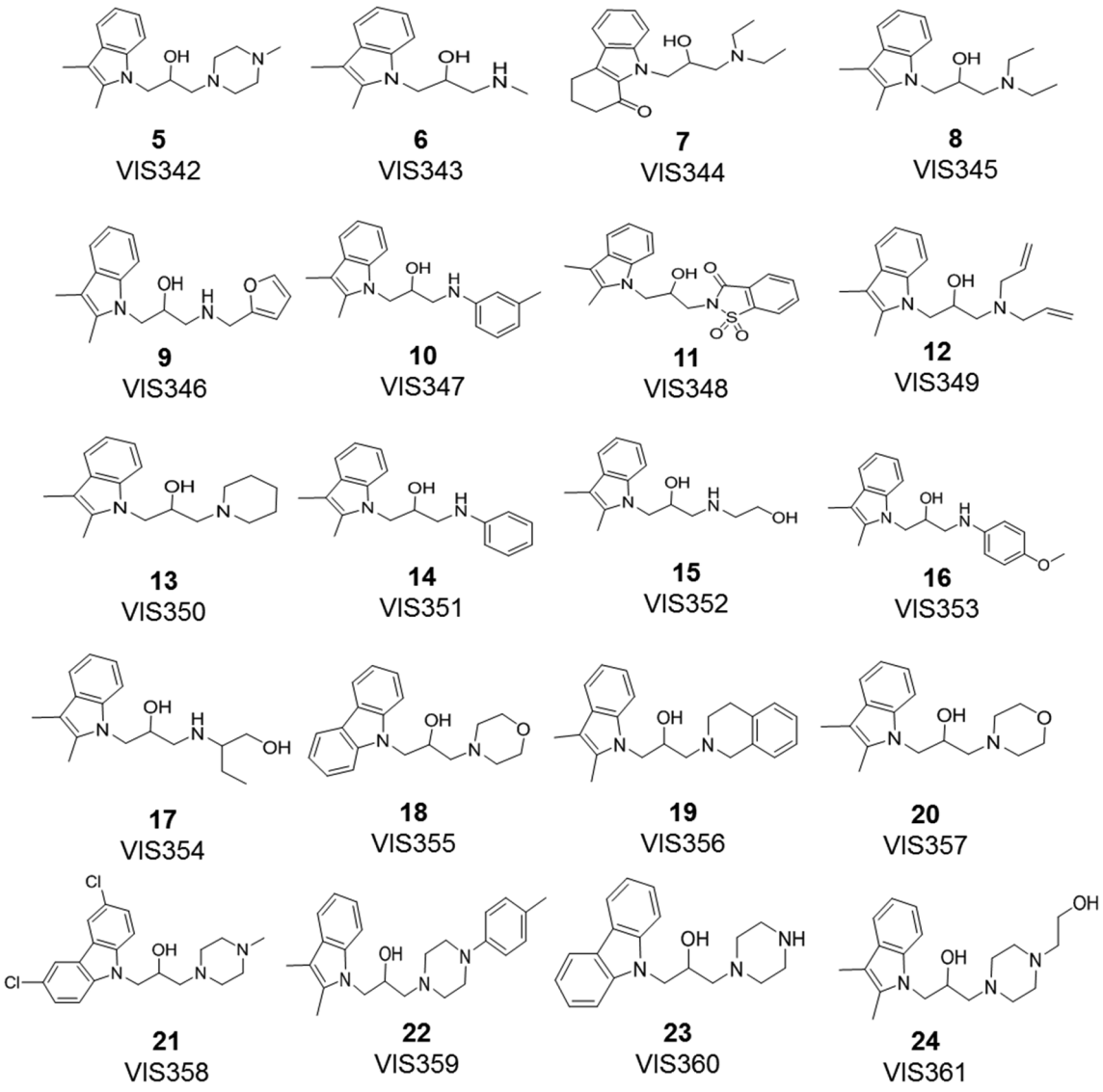

Fig. 3. Chemical structures of VIS237 analogues (**5–24**).

14, hereafter indicated as VIS351, which demonstrated a safe profile in addition to a high CS score. We thus determined the IC_{50} value of VIS351 by building a dose–response curve in the cellular assay. VIS351 was 3-fold diluted starting from its highest non-cytotoxic concentration (90 μM), whereas NLG919 was 3-fold diluted from 0.1 μM. The obtained curves of concentration provided a cellular IC_{50} = 11.463 ± 6.323 μM and IC_{50} = 0.013 ± 0.003 μM for VIS351 and the reference inhibitor NLG919, respectively (Fig. 5B). In order to verify the specificity of the IDO1 inhibitory activity of VIS351, we tested the molecule in the same cell line stably expressing the mouse TDO, instead of IDO1. The cellular test demonstrated a dose-dependent inhibition of Kyn production by P1.IDO1 but not P1.TDO cells (Fig. 5C).

Next we performed a biochemical assay [30,37] to determine the enzymatic IC_{50} of VIS351 on the isolated recombinant IDO1 protein. We conducted the assay by using seven times 10-fold dilutions of the molecule, starting from the highest soluble concentration (2 mM). As expected, the reference inhibitor NLG919 showed a low enzymatic IC_{50} = 0.518 ± 0.060 μM, whereas VIS351 did not inhibit the catalytic activity of the recombinant IDO1 at any tested concentrations (Fig. 5D). Therefore and unexpectedly, we could not determine an enzymatic IC_{50} for the novel compound, although the molecule had demonstrated a strong binding activity in MST experiments performed on the same protein target. The above observations suggested that, despite a strong binding of the IDO1 protein and inhibition of Kyn production by P1.IDO1 cells, VIS351 fails to act as a catalytic inhibitor of the recombinant IDO1 protein.

3.4. Binding mode of VIS351 molecule

In addition to the catalytic activity of IDO1, we previously identified and characterized a function of the protein mediated by two highly conserved ITIM-1 and ITIM-2 motifs, which, once phosphorylated, promote a fine modulation of the protein expression [20,22] and confer a long-term immunoregulatory phenotype in different subsets of DCs [21,38,39]. Moreover, we demonstrated that the folding conformation of IDO1 necessary for mediating the ITIMs functions is not compatible with the one required for the catalytic activity, since the negative charge carried by phosphorylated tyrosines in ITIMs may affect the shape of the catalytic site. Therefore, a dynamic balance between the two IDO1 conformations that seem to be mutually exclusive may occur [23]. We thus applied a molecular docking to investigate the binding mode of VIS351, attempting to envisage any relationship between molecular interactions of the ligand into the catalytic pocket and the ITIM's tyrosines. Docking studies of this ligand into the catalytic cleft of IDO1 provided two solutions depicting similar binding poses with very similar energetical scores (solution #1: XPscore = −8.4 kcal/mol;

Table 2
List of molecular fragments used in this study.

Compound	Code	MW	MST K_d (μM)	BEI
2	NLG919	282	3.3 ± 0.4	19
5	VIS342	301.4	256.5 ± 74.4	12
6	VIS343	232.3	243.8 ± 71.9	16
7	VIS344	314.4	653.5 ± 110.6	10
8	VIS345	274.4	> 1000	–
9	VIS346	298.4	102.5 ± 13.4	13
10	VIS347	308.4	> 1000	–
11	VIS348	384.4	404.8 ± 139.8	9
12	VIS349	298.4	302.0 ± 107.0	12
13	VIS350	286.4	6.3 ± 2.0	18
14	VIS351	294.4	1.9 ± 0.7	19
15	VIS352	262.4	580.0 ± 123.6	12
16	VIS353	324.4	59.5 ± 6.5	13
17	VIS354	290.4	294.0 ± 124.0	12
18	VIS355	310.4	13.4 ± 6.2	16
19	VIS356	334.5	118.5 ± 19.1	12
20	VIS357	302.4	13.1 ± 6.8	16
21	VIS358	392.3	1.5 ± 0.32	15
22	VIS359	377.5	4.0 ± 0.8	14
23	VIS360	309.4	> 1000	–
24	VIS361	365.9	> 1000	–

Abbreviations: MW, molecular weight. MST, microscale thermophoresis. BEI, binding efficiency index.

solution #2: XPscore = −8.2 kcal/mol) (Fig. 6A and B). In both solutions, VIS351 did not engage the heme group with hydrogen bonds and/or coordinative interactions, but only the two methyl groups of the indole moiety could make hydrophobic contacts with the porphyrin ring. Aromatic interactions were present between the indole moiety of this compound and the side chains of Tyr126, Phe163, Phe164, and Phe226 in both binding poses. Likewise, the terminal aromatic ring of VIS351 (**14**) was positioned close to Arg231, suggesting the formation of π-cation interactions. The difference between the two binding poses was determined by the polar group of the ligand engaging Gly262 in a hydrogen bond. In the first solution, the hydroxyl group of the central propanol scaffold interacted with the carbonyl group of Gly262. Conversely, the second solution showed the aniline nitrogen engaging Gly262 with a hydrogen bond. According to molecular docking results, it is worth noting that no direct interaction were observed between VIS351 and the ITIM's tyrosines (Tyr111, Tyr249), which are located 20 Å away from the center of mass of ligand (Fig. 6C). However, the lack of a strong polar interaction between the molecule and the heme cofactor may bestow higher plasticity on the ligand-bound complex, allowing a conformational shift toward an ITIM-favoring form of IDO1 with the detriment of its enzymatically active conformation, thus resulting in Kyn reduction as we observed in the cellular assay.

Embracing the hypothesis that the plasticity of VIS351-bound IDO1 could affect an ITIM-favoring conformation of IDO1, we next studied

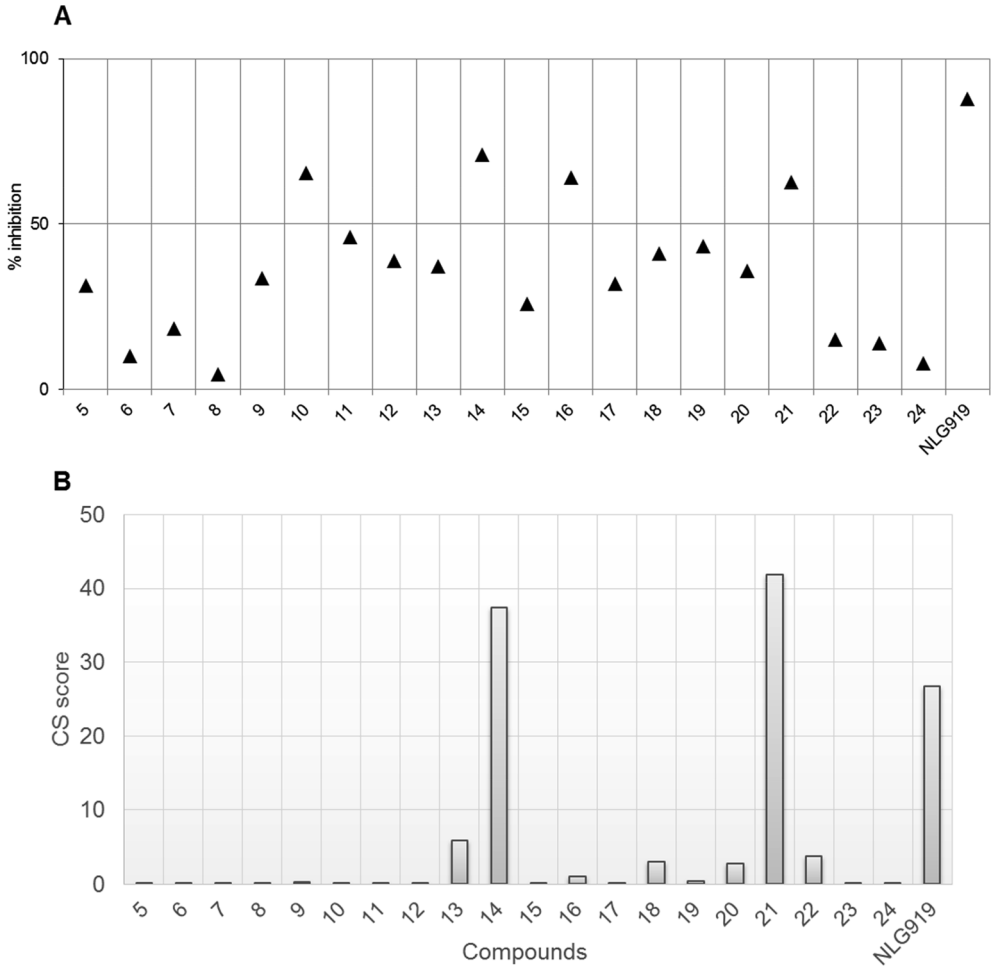

Fig. 4. A) Percentage of inhibition of Kyn production by P1.IDO1 cells after treatment with the molecular fragments or DMSO (vehicle), as control. The NLG919 analogue represents the reference inhibitor. Results are the mean of three experiments conducted in triplicate. B) The combined screening (CS) score of each compound, calculated as the ratio between the percentage of inhibition resulting from the cellular assay and the K_d value (μM) was measured by MST.

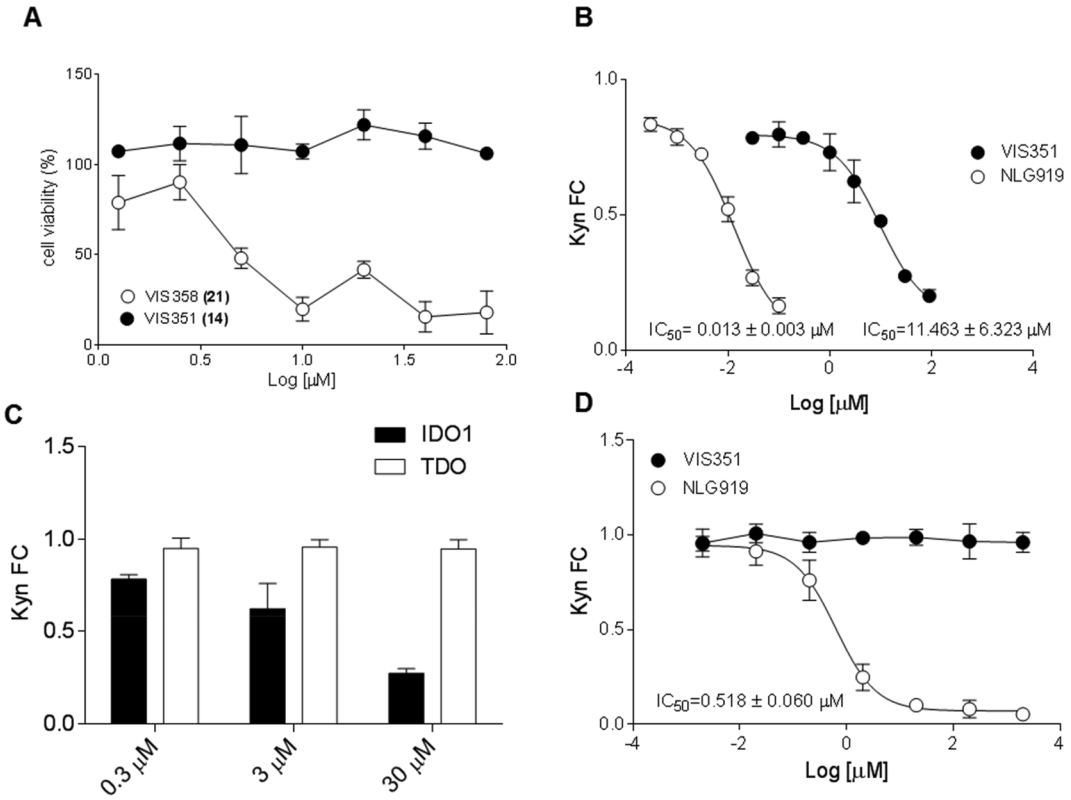

Fig. 5. A) Concentration-dependent cytotoxicity of VIS351 (**14**, filled circle) and VIS358 (**21**, open circle) in P1.IDO1 cells. Cell viability percentage (%) is represented as the mean ± SD of three experiments conducted in triplicate. B) Cellular IC_{50} value (μM) of VIS351 (**14**, filled circle) and NLG919 (as reference inhibitor, open circle) obtained from a dose–response curve. P1.IDO1 cells were exposed to six times 3-fold serial dilutions of NLG919 (concentrations ranging from 0.0003 to 0.1 μM) and eight times 3-fold serial dilutions of VIS351 (concentrations ranging from 0.03 to 90 μM). Results are the mean ± SD of the Kyn fold change (Kyn FC) of three independent experiments, each performed in triplicate. C) Kyn FC in the supernatants from P1.IDO1 (filled bar) and P1.TDO (open bar) cells incubated with three different 10-fold dilutions of VIS351. Results represent the mean ± SD from three independent experiments. D) Enzymatic IC_{50} of VIS351 (**14**, filled circle) and NLG919 (open circle) are determined on recombinant human IDO1, using seven times 10-fold dilutions of the molecules, starting from 2 mM. Kyn FC values are represented as the mean ± SD of three independent experiments, each performed in triplicate.

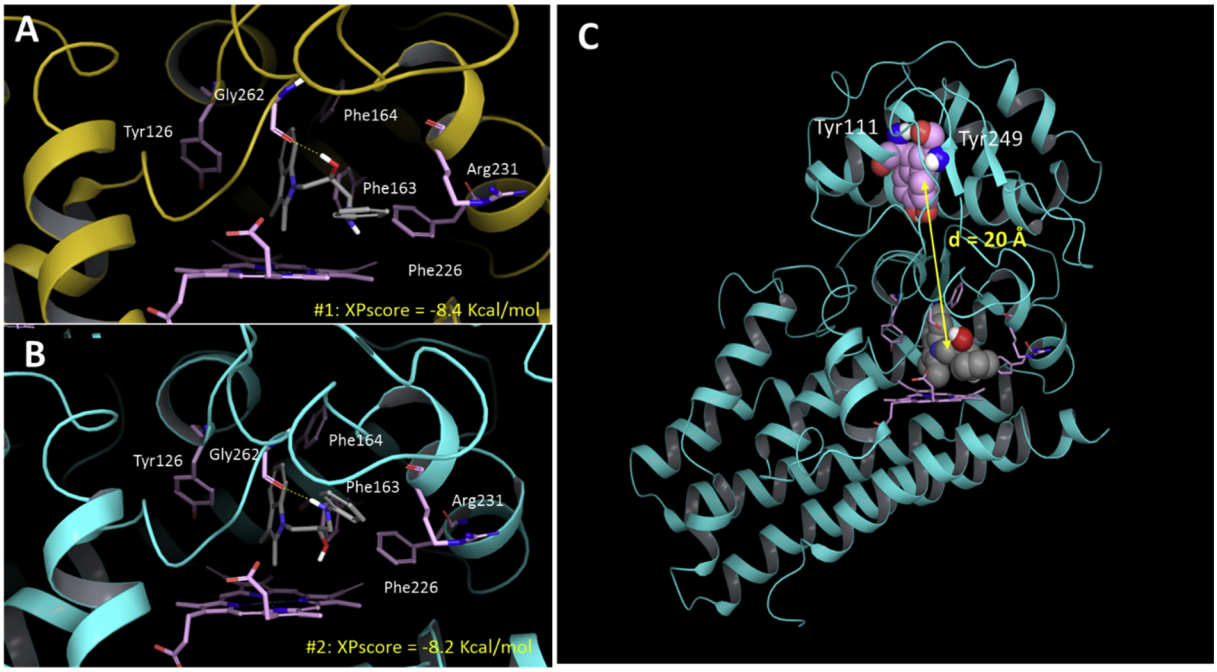

Fig. 6. Top scored binding pose (A; solution #1) and second ranked binding pose of VIS351 (**14**) from docking study (B; solution #2). C) Distance (d) between the center of mass of VIS351 (**14**) and the center of mass of Tyr111 and Tyr249 residues, contained in ITIM-1 and ITIM-2 of IDO1 protein, respectively.

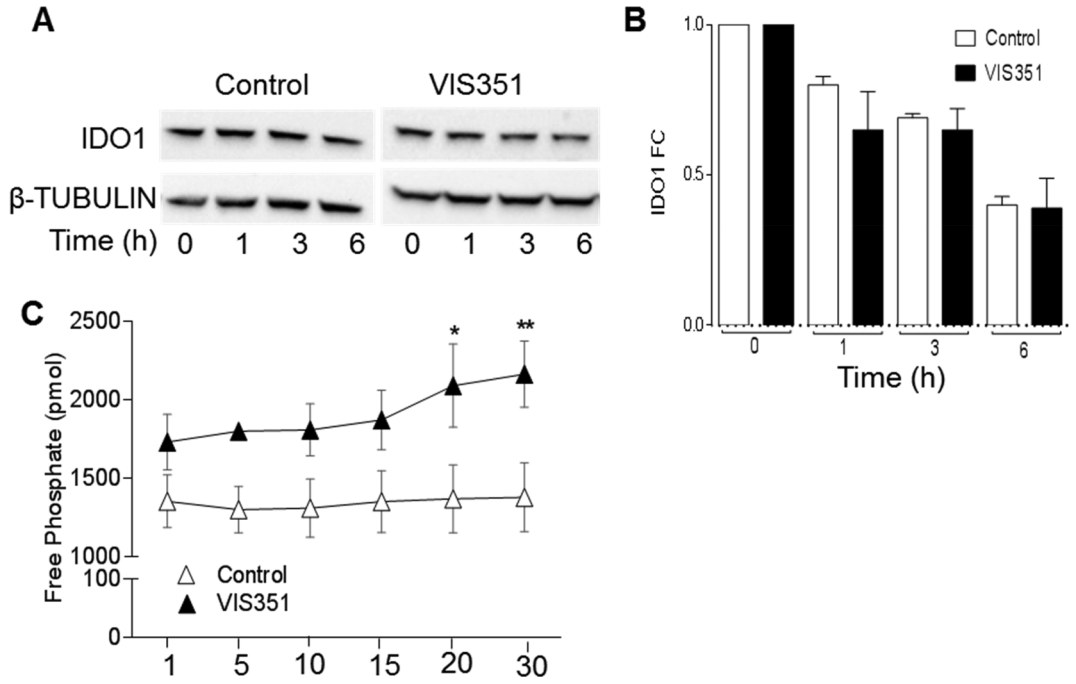

Fig. 7. A) IDO1 protein expression in P1.IDO1 cells treated with 30 μM of VIS351 (**14**) or vehicle at the indicated time-points (0–6 h). Whole cell lysates were subjected to immunoblot analysis, using an IDO1-specific antibody. Detection of β-tubulin served as a loading control. One representative experiment is shown. B) Kinetics of IDO1 protein degradation in P1.IDO1 cells treated with VIS351 (filled bar) or vehicle (open bar) for 0, 1, 3 and 6 h. A quantitative analysis of three independent experiments (mean ± SD) of Western blot analysis is represented as the ratio of normalized IDO1 protein at each time point (1, 3 and 6 h) over time 0. C) Phosphatase activity produced by IDO1 immunoprecipitated from untreated (open triangle) and VIS351-treated (filled triangle) P1.IDO1. Levels of free phosphate (pmol) generated during the incubation of a tyrosine-phosphorylated peptide with the co-immunoprecipitated IDO1 proteins from each condition. Results are representative of three independent experiments (mean ± SEM). $^{*}p < 0.05$, $^{**}p < 0.01$, VIS351-treated versus DMSO-treated P1.IDO1 cells (Paired Student's *t*-test).

the effects of VIS351 on the ITIM-mediated functions of the enzyme.

3.5. VIS351 promotes the ITIM-mediated signaling activity of IDO1

We previously demonstrated that the ITIM-mediated activity of IDO1 can affect the half-life of the protein, by triggering the proteasomal degradation or the *de novo* synthesis of IDO1 as a consequence of the association of the phosphorylated IDO1's ITIMs with different protein partners, namely SOCS3 or SHP-1 and SHP-2 phosphatases, respectively [22]. We thus investigated whether VIS351 could affect either the ITIM-mediated mechanisms of IDO1. To this purpose, after protein translational inhibition by cycloheximide, we subjected P1.IDO1 cells to treatment for 0–6 h with 30 μM of VIS351 or DMSO, as control, and analyzed the expression of the IDO1 protein over time. As expected, we found a gradual reduction of β-tubulin-normalized IDO1 expression in the control lysates, reaching a decrease of 60% in 6 h. In a similar manner, the turnover of the IDO1 protein in VIS351-treated P1.IDO1 cells overlapped the pattern observed in the control, indicating that VIS351 may not affect the ITIM-mediated mechanism of the proteasomal degradation of IDO1 (Fig. 7A and B).

We next investigated the modulation of IDO1 association with tyrosine phosphatases by VIS351, by evaluating the ability of IDO1 immunoprecipitates to remove a phosphate group from a tyrosine-phosphorylated substrate, as described [21,23]. Specifically, we quantified the amount of free phosphate produced over 30 min by IDO1 immunoprecipitated from untreated and VIS351-treated P1.IDO1 cells. As previously shown [23], we observed a basal phosphatase activity associated with IDO1 immunoprecipitates obtained from P1.IDO1 cells. However, preconditioning of P1.IDO1 cells with VIS351 for 4 h generated a significantly increased level of free phosphate at 20 min of the colorimetric reaction, as compared to control (Fig. 7C), highlighting an interesting effect of VIS351 in promoting an alternative conformation of IDO1 suitable to acquire the capacity to interact with tyrosine phosphatases.

3.6. VIS351 confers an immunosuppressive phenotype on pDCs detectable in vivo

ITIM-related functions of IDO1 were firstly described in DCs, which are characterized by a plastic phenotype prompt to respond to whichever environmental signals [20,21]. pDCs represent the most flexible DC subset that can shift from an immunostimulatory toward an immunosuppressive program for rapidly and efficiently sensing the extracellular milieu [40]. In order to better understand the biological relevance of VIS351, as a positive modulator of the signaling conformation of IDO1, we evaluated the *in vivo* priming ability of pDCs after *in vitro* conditioning with VIS351. Specifically, we sensitized female mice with the *H-2*D^b–restricted HY peptide presented by a combination of immunogenic cDCs and a minority fraction of pDCs pre-incubated *in vitro* overnight with VIS351 or DMSO, as control. Two weeks later, we evaluated the antigen-specific reactivity through an intrafootpad challenge of the HY antigen, according to an established protocol for measuring the induction of immune reactivity versus tolerance [41–44]. As expected, sensitization of mice with a combination of immunogenic cDCs and vehicle-treated pDCs elicited a positive response against the HY antigen in mice. In contrast, VIS351-pretreated pDCs abrogated the immunoadjuvant response elicited by cDCs, suggesting that VIS351 could induce in pDCs a tolerogenic phenotype. Moreover, preconditioning of *Ido1*$^{-/-}$ pDCs with VIS351 in the same *in vivo* assay negated the tolerogenic properties in pDCs that evidently would require an intact IDO1 protein to mediate VIS351-induced immunosuppression *in vivo* (Fig. 8A).

We previously demonstrated that the ITIM-mediated signaling activity of IDO1 in pDCs triggers a positive loop culminating in a late

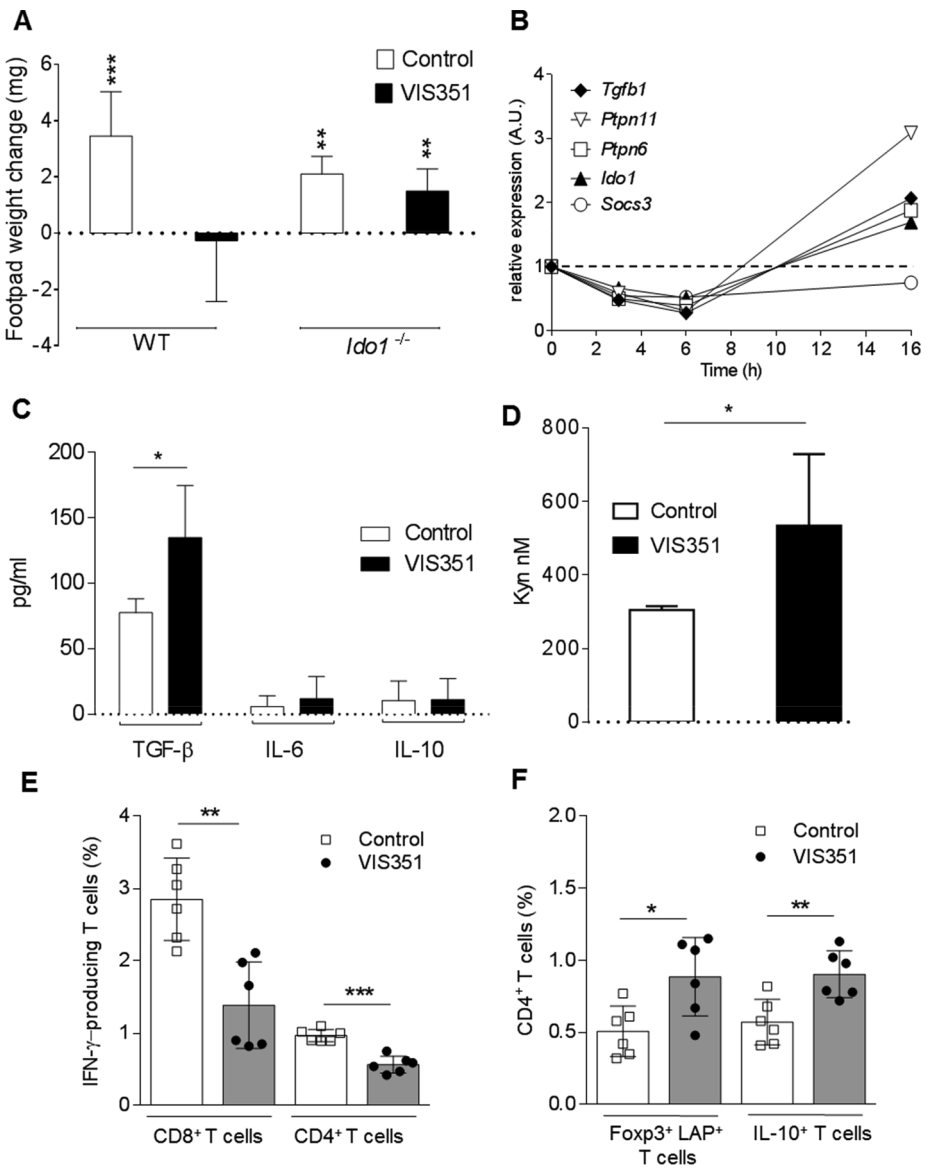

Fig. 8. A) Skin test reactivity of mice immunized with pDCs treated with VIS351 (filled bar) or vehicle (open bar). Splenic HY-pulsed cDCs in combination with a minority fraction (5%) of WT or *Ido1*$^{-/-}$ pDCs were transferred into syngeneic C57BL/6 recipient female mice to be assayed for skin reactivity to the eliciting peptide. Skin reactivity of the recipient mice (n = 6 per group) to the eliciting peptide is represented as change in the footpad weight. Results are representative of two independent experiments (mean ± SD). $^{**}p < 0.01$; $^{***}p < 0.001$. The significance marked on the histograms is referred to a two-tailed paired Student's *t* test (experimental vs control footpads) in each group of mice. B) Gene transcription of *Ido1, Tgfb1, Ptpn6, Ptpn11* and *Socs3* in pDCs treated with 30 μM of VIS351 or vehicle for 0, 3, 6 and 16 h. Data represent the fold change expression of *Gapdh*-normalized transcripts in VIS351-treated pDCs relative to vehicle-treated cells for each time point. Results represent the mean of three different experiments and the dotted line denotes a FC = 1. C) Secretion of TGF-β, IL-6, and IL-10 in supernatants of pDCs treated *in vitro* with 30 μM of VIS351 (filled bar) or vehicle (open bar). Results are the mean ± SD from three different experiments. $^{*}p < 0.05$ (Student's *t*-test). D) Kyn production in the culture supernatants of untreated (open bar) and VIS351 treated-pDCs (filled bar) *in vitro* incubated for 16 h. Results are the mean ± SD from three different experiments. $^{*}p < 0.05$ (Student's *t*-test). E) IFN-γ-producing CD3^{+} CD44^{+} T cells frequencies in draining lymph nodes from mice immunized with pDCs treated with VIS351 (filled bar) or vehicle as control (open bar). Data represent the mean ± SD; $n = 6$. $^{*}p < 0.05$, $^{**}p < 0.01$, $^{***}p < 0.001$ (Student's *t*-test). F) Frequency of CD4^{+}CD44^{+} T cells expressing Foxp3 and LAP or IL-10 in draining lymph nodes from mice immunized with pDCs treated with VIS351 (filled bar) or vehicle as control (open bar). Data represent mean ± SD; $n = 6$. $^{*}p < 0.05$, $^{**}p < 0.01$ (Student's *t*-test).

induction of the immunoregulatory cytokine TGF-β and the IDO1 itself, both responsible for a long-term immunoregulatory phenotype of the pDCs [21,31,45]. Thus, in pDCs treated with VIS351, we monitored over time the gene transcription of key molecules involved in such self-maintaining regulatory circuitry, including *Ido1, Tgfb1* (coding for the immunoregulatory cytokine TGF-β), *Ptpn6 and Ptpn11* (coding for SHP-1 and SHP-2 phosphatases, respectively). We did not observe any early induction of the examined genes in the first 6 h of pDC stimulation with VIS351, but we did detect a late induction of the above genes after 16 h of stimulation. Conversely, expression of *Socs3* in the same cells was not affected by VIS351 treatment at any time points, thus excluding the occurring of the alternative ITIM-mediated function of IDO1 that leads to its proteasomal degradation [20,22] (Fig. 8B).

A late gene induction of the molecular players participating in the signaling activity of IDO1 suggested that VIS351 may indirectly promote the induction of such molecules, by favoring a conformation of the IDO1 protein suitable for the activation of the ITIM-mediated signaling mechanism, as already suggested by the cellular and the enzymatic screenings. In addition, VIS351 also induced a significantly increased level of the immunoregulatory cytokine TGF-β but not of the proinflammatory cytokine IL-6 which drives the ITIM-mediated proteasomal degradation of IDO1 [20]. Nor IL-10 (Fig. 8C) neither TNF-α or IFN-α (data not shown) levels were affected by VIS351 in pDCs, suggesting a priority role of the immunoregulatory cytokine TGF-β in the VIS351-induced activity of IDO1 protein. More interestingly, VIS351 significantly induced the secretion of Kyn in pDCs (Fig. 8D), possibly representing a downstream event triggered by activation of the signaling function of IDO1 that can induce its own expression in pDCs, thus promoting a tolerogenic phenotype in the cells [21].

By cytofluorometric analysis of popliteal lymph node cells (i.e., draining antigen-challenged footpads), we found that the abrogation of skin test reactivity elicited by VIS351-treated pDCs was accompanied by significantly decreased frequencies of IFN-γ-producing CD8^{+} and CD4^{+} T cells (Fig. 8E), when compared to the control group with detectable skin reactivity. A significant increase of CD4^{+} T cells expressing surface TGF-β in its LAP form and the transcription factor Foxp3 as well as of IL-10-producing CD4^{+} T cells was also found (Fig. 8F). Overall, the phenotypic characterization of the main T cell subsets populating the antigen-draining lymph nodes of mice sensitized with VIS351-treated pDCs suggested the possible instauration of an immunoregulatory microenvironment that would oppose the migration of IFN-γ−producing CD8^{+} and CD4^{+} T cells.

Thus activation of the ITIM-based signaling function of IDO1 by VIS351 in pDCs may trigger a self-maintained immunoregulatory

circuitry *in vivo* where TGF-β plays a dominant role during the antigen-specific immune response. TGF-β may be indeed at work in the afferent phase of sensitization by VIS351-treated pDCs, which secrete higher levels of TGF-β, and also in the later efferent phase of antigen recalling response, where regulatory T cell would contribute to maintain high the levels of the cytokine.

4. Discussion

Since its identification as a critical enzyme in cancer's evasion of immune responses [46], drug discovery efforts have been intensively pursued to develop effective and selective catalytic inhibitors of IDO1. IDO1 is now considered an immune checkpoint molecule [47] and thus IDO1 targeting has become an attractive approach in immuno-oncology. Differently from immune checkpoint receptors (i.e., CTLA-4 and PD-1) expressed on the cell membrane and easily accessible by specific antibodies, IDO1 is an intracellular enzyme, best druggable by small molecules. To date, the majority of IDO1-specific molecules acts as competitive or noncompetitive inhibitors, by either mimicking the tryptophan substrate or by binding the heme cofactor, respectively [48]. Although IDO1 inhibitors are largely recognized as powerful 'immunometabolic adjuvants' to enhance anti-tumor immune responses—at least in preclinical models [49] — epacadostat recently showed disappointing efficacy in cancer's patients in combination with pembrolizumab, an anti-PD-1 antibody [50,51]. As a consequence of this failure, other clinical trials with IDO1 inhibitors have been suspended, canceled, or downsized. Although several reasons may explain epacadostat's results, further studies on the basic biology of the enzyme may be mandatory to unravel the complex IDO1-driven immunoregulatory network.

In addition to impairing immune effector functions via tryptophan starvation, IDO1 (and TDO) catalyzes the formation of Kyn that also mediates tumor immune escape mechanisms via activation of AhR. Interestingly, Liu Y et al. recently identified a Kyn-AhR-dependent mechanism upregulating PD-1 in tumor-specific cytotoxic T lymphocytes and thus promoting immune escape [52]. These data would support the rationale of combining IDO1 inhibitors with PD-1-specific antibodies. Nevertheless, the failure of phase III trial with Incyte's epacadostat and Merck & Co's pembrolizumab would suggest the existence of additional causes impairing therapeutic efficacy. A confounding factor of this history is the recent observation that some IDO1 inhibitors (i.e., epacadostat and NLG919A) bind the AhR and, on their own, could suppress the immune system, thus inducing the opposite outcome of the drug's intent [53]. How much such 'off-target' effects may reverberate on the anti-tumor efficacy of IDO1 inhibitors is still unclear. However, it should be kept into consideration for the optimization of pharmaceutical properties of this class of drugs.

A further grade of complexity in considering IDO1 as a drug target consists in its 'moonlighting' feature that confers a unique multi-tasking functional profile. Two different activities reside in the monomeric IDO1 protein, i.e., the well-characterized catalytic function that requires the heme cofactor in the large domain of the protein [25] and the most recent signaling function of IDO1 requiring the tyrosine-phosphorylation of ITIM-1 and ITIM-2 motifs located in the small domain [20,21]. Major conformational changes may occur in IDO1 protein in order to expose ITIM's phosphorylable tyrosines and activate the ITIM-mediated activity. The negative charge carried by phosphorylated tyrosines of ITIMs may affect the shape of the catalytic site, so that the ITIM-favoring conformation would exclude the catalytic active form of IDO1 [23]. The characterization of VIS351 as a modulator of the ITIM-mediated signaling of IDO1, rather than its catalytic activity, identifies for the first time a molecule acting on the non-enzymatic activity of IDO1 and paves the basis for a novel screening approach of molecules targeting the ITIM functions of IDO1. On one hand, because IDO1 catalytic inhibitors have failed in cancer clinical setting, the molecular dissection of the ITIM signaling pathway in DCs may provide further therapeutic opportunities to make IDO1 protein an effective drug target. On the other hand, reinterpreting the clinical failure of IDO1 inhibitors under the lens of the ITIM-mediated signaling in DCs may suggest innovative immunotherapeutic combinations. In fact, it should be underlined that the IDO1 ITIM-mediated signaling sustains a long-term immunoregulatory circuitry in DCs that may restrain abnormal immune responses [31]. Beyond its role as immune checkpoint inhibitor to be blocked in cancer, IDO1 could be conversely exploited in a variety of immune disorders, including autoimmune diabetes [47], where the enzyme has been demonstrated to be defective in both the preclinical models [11,15] and the human disease [54,55]. To date, positive modulators of IDO1 (i.e., catalytic enhancer as well as allosteric modulators of IDO1 signaling) are lacking and therefore, VIS351 may represent an important compound capable of bridging such gap.

Overall, the dual regulatory function of IDO1, as a catalyst and a signaling molecule, makes this protein a fascinating immunotherapeutic target. Positive modulators of the ITIM-mediated activity of IDO1 may come as a breath of fresh air in IDO1-based drug discovery.

Acknowledgments

This work was supported by the Italian Ministry of Education, Universities and Research, Italy (PRIN2012-2012S47X27 to CO and AM) and by the European Research Council, FP7 EU (338954_DIDO to UG and AM).

Conflict of interest

The authors declare that they have no conflicts of interest with the contents of this article.

Author contributions

CO and AM designed the study and wrote the paper. FG performed docking studies and purchased the molecules. AC performed thermophoresis analyses. EA, MTP, MLB designed and performed *in vitro* experiments and analyzed the data. CV, GM and RB performed *in vivo* experiments. MG performed flow cytometry analysis. CO and UG supervised the experiments. All authors reviewed results and approved the final version of the manuscript.

References

[1] F. Fallarino, U. Grohmann, S. You, B.C. McGrath, D.R. Cavener, C. Vacca, C. Orabona, R. Bianchi, M.L. Belladonna, C. Volpi, M.C. Fioretti, P. Puccetti, Tryptophan catabolism generates autoimmune-preventive regulatory T cells, Transpl. Immunol. 17 (1) (2006) 58–60.
[2] P. Puccetti, F. Fallarino, Generation of T cell regulatory activity by plasmacytoid dendritic cells and tryptophan catabolism, Blood Cells Mol. Dis. 40 (1) (2008) 101–105.
[3] F. Fallarino, U. Grohmann, S. You, B.C. McGrath, D.R. Cavener, C. Vacca, C. Orabona, R. Bianchi, M.L. Belladonna, C. Volpi, P. Santamaria, M.C. Fioretti, P. Puccetti, The combined effects of tryptophan starvation and tryptophan catabolites down-regulate T cell receptor zeta-chain and induce a regulatory phenotype in naive T cells, J. Immunol. (Baltimore, Md.: 1950) 176 (11) (2006) 6752–6761.
[4] Y.H. Ryu, J.C. Kim, Expression of indoleamine 2,3-dioxygenase in human corneal cells as a local immunosuppressive factor, Invest. Ophthalmol. Vis. Sci. 48 (9) (2007) 4148–4152.
[5] P. Sedlmayr, A. Blaschitz, R. Stocker, The role of placental tryptophan catabolism, Front. Immunol. 5 (2014) 230.
[6] S.A. Sarkar, R. Wong, S.I. Hackl, O. Moua, R.G. Gill, A. Wiseman, H.W. Davidson, J.C. Hutton, Induction of indoleamine 2,3-dioxygenase by interferon-gamma in human islets, Diabetes 56 (1) (2007) 72–79.
[7] A.W. Yeung, A.C. Terentis, N.J. King, S.R. Thomas, Role of indoleamine 2,3-dioxygenase in health and disease, Clin. Sci. (Lond.) 129 (7) (2015) 601–672.
[8] L. Romani, F. Fallarino, A. De Luca, C. Montagnoli, C. D'Angelo, T. Zelante, C. Vacca, F. Bistoni, M.C. Fioretti, U. Grohmann, B.H. Segal, P. Puccetti, Defective tryptophan catabolism underlies inflammation in mouse chronic granulomatous disease, Nature 451 (7175) (2008) 211–215.
[9] U. Grohmann, C. Orabona, F. Fallarino, C. Vacca, F. Calcinaro, A. Falorni, P. Candeloro, M.L. Belladonna, R. Bianchi, M.C. Fioretti, P. Puccetti, CTLA-4-Ig

regulates tryptophan catabolism in vivo, Nat. Immunol. 3 (11) (2002) 1097–1101.
[10] A. Staudacher, T. Hinz, N. Novak, D. von Bubnoff, T. Bieber, Exaggerated IDO1 expression and activity in Langerhans cells from patients with atopic dermatitis upon viral stimulation: a potential predictive biomarker for high risk of Eczema herpeticum, Allergy 70 (11) (2015) 1432–1439.
[11] U. Grohmann, F. Fallarino, R. Bianchi, C. Orabona, C. Vacca, M.C. Fioretti, P. Puccetti, A defect in tryptophan catabolism impairs tolerance in nonobese diabetic mice, J. Exp. Med. 198 (1) (2003) 153–160.
[12] J.E. Cheong, L. Sun, Targeting the IDO1/TDO2-KYN-AhR pathway for cancer immunotherapy – challenges and opportunities, Trends Pharmacol. Sci. (2017).
[13] M. El-Zaatari, A.J. Bass, R. Bowlby, M. Zhang, L.J. Syu, Y. Yang, H. Grasberger, A. Shreiner, B. Tan, S. Bishu, W.K. Leung, A. Todisco, N. Kamada, M. Cascalho, A.A. Dlugosz, J.Y. Kao, Indoleamine 2,3-dioxygenase 1, increased in human gastric pre-neoplasia, promotes inflammation and metaplasia in mice and is associated with type II hypersensitivity/autoimmunity, Gastroenterology 154 (1) (2018) 140–153.e17.
[14] J.P. Chalise, M.T. Pallotta, IDO1 and TGF-beta mediate protective effects of IFN-alpha in antigen-induced, Arthritis 197 (8) (2016) 3142–3151.
[15] G. Mondanelli, E. Albini, M.T. Pallotta, C. Volpi, L. Chatenoud, C. Kuhn, F. Fallarino, D. Matino, M.L. Belladonna, R. Bianchi, C. Vacca, S. Bicciato, L. Boon, G. Ricci, U. Grohmann, P. Puccetti, C. Orabona, The proteasome inhibitor bortezomib controls indoleamine 2,3-dioxygenase 1 breakdown and restores immune regulation in autoimmune diabetes, Front. Immunol. 8 (2017) 428.
[16] N.T. Nguyen, A. Kimura, T. Nakahama, I. Chinen, K. Masuda, K. Nohara, Y. Fujii-Kuriyama, T. Kishimoto, Aryl hydrocarbon receptor negatively regulates dendritic cell immunogenicity via a kynurenine-dependent mechanism, PNAS 107 (46) (2010) 19961–19966.
[17] J.D. Mezrich, J.H. Fechner, X. Zhang, B.P. Johnson, W.J. Burlingham, C.A. Bradfield, An interaction between kynurenine and the aryl hydrocarbon receptor can generate regulatory T cells, J. Immunol. (Baltimore, Md.: 1950) 185 (6) (2010) 3190–3198.
[18] F. Fallarino, U. Grohmann, C. Vacca, R. Bianchi, C. Orabona, A. Spreca, M.C. Fioretti, P. Puccetti, T cell apoptosis by tryptophan catabolism, Cell Death Differ. 9 (10) (2002) 1069–1077.
[19] M.L. Belladonna, C. Orabona, U. Grohmann, P. Puccetti, TGF-beta and kynurenines as the key to infectious tolerance, Trends Mol. Med. 15 (2) (2009) 41–49.
[20] C. Orabona, M.T. Pallotta, C. Volpi, F. Fallarino, C. Vacca, R. Bianchi, M.L. Belladonna, M.C. Fioretti, U. Grohmann, P. Puccetti, SOCS3 drives proteasomal degradation of indoleamine 2,3-dioxygenase (IDO) and antagonizes IDO-dependent tolerogenesis, PNAS 105 (52) (2008) 20828–20833.
[21] M.T. Pallotta, C. Orabona, C. Volpi, C. Vacca, M.L. Belladonna, R. Bianchi, G. Servillo, C. Brunacci, M. Calvitti, S. Bicciato, E.M. Mazza, L. Boon, F. Grassi, M.C. Fioretti, F. Fallarino, P. Puccetti, U. Grohmann, Indoleamine 2,3-dioxygenase is a signaling protein in long-term tolerance by dendritic cells, Nat. Immunol. 12 (9) (2011) 870–878.
[22] C. Orabona, M.T. Pallotta, U. Grohmann, Different partners, opposite outcomes: a new perspective of the immunobiology of indoleamine 2,3-dioxygenase, Mol. Med. 18 (2012) 834–842.
[23] E. Albini, V. Rosini, M. Gargaro, G. Mondanelli, M.L. Belladonna, M.T. Pallotta, C. Volpi, F. Fallarino, A. Macchiarulo, C. Antognelli, R. Bianchi, C. Vacca, P. Puccetti, U. Grohmann, C. Orabona, Distinct roles of immunoreceptor tyrosine-based motifs in immunosuppressive indoleamine 2,3-dioxygenase 1, J. Cell Mol. Med. 21 (1) (2017) 165–176.
[24] S. Duhr, D. Braun, Why molecules move along a temperature gradient, PNAS 103 (52) (2006) 19678–19682.
[25] A. Coletti, F. Camponeschi, E. Albini, F.A. Greco, V. Maione, C. Custodi, F. Ianni, U. Grohmann, C. Orabona, F. Cantini, A. Macchiarulo, Fragment-based approach to identify IDO1 inhibitor building blocks, Eur. J. Med. Chem. 141 (2017) 169–177.
[26] C. Abad-Zapatero, Ligand efficiency indices for effective drug discovery, Expert Opin. Drug Discov. 2 (4) (2007) 469–488.
[27] Y.H. Peng, S.H. Ueng, C.T. Tseng, M.S. Hung, J.S. Song, J.S. Wu, F.Y. Liao, Y.S. Fan, M.H. Wu, W.C. Hsiao, C.C. Hsueh, S.Y. Lin, C.Y. Cheng, C.H. Tu, L.C. Lee, M.F. Cheng, K.S. Shia, C. Shih, S.Y. Wu, Important hydrogen bond networks in indoleamine 2,3-dioxygenase 1 (IDO1) inhibitor design revealed by crystal structures of imidazoleisoindole derivatives with IDO1, J. Med. Chem. 59 (1) (2016) 282–293.
[28] H.M. Berman, J. Westbrook, Z. Feng, G. Gilliland, T.N. Bhat, H. Weissig, I.N. Shindyalov, P.E. Bourne, The protein data bank, Nucl. Acids Res. 28 (1) (2000) 235–242.
[29] F. Fallarino, C. Uyttenhove, T. Boon, T.F. Gajewski, Endogenous IL-12 is necessary for rejection of P815 tumor variants in vivo, J. Immunol. (Baltimore, Md.: 1950) 156 (3) (1996) 1095–1100.
[30] C.J. Austin, J. Mizdrak, A. Matin, N. Sirijovski, P. Kosim-Satyaputra, R.D. Willows, T.H. Roberts, R.J. Truscott, G. Polekhina, M.W. Parker, J.F. Jamie, Optimised expression and purification of recombinant human indoleamine 2,3-dioxygenase, Protein Expr. Purif. 37 (2) (2004) 392–398.
[31] M.T. Pallotta, C. Orabona, R. Bianchi, C. Vacca, F. Fallarino, M.L. Belladonna, C. Volpi, G. Mondanelli, M. Gargaro, M. Allegrucci, V.N. Talesa, P. Puccetti, U. Grohmann, Forced IDO1 expression in dendritic cells restores immunoregulatory signalling in autoimmune diabetes, J. Cell Mol. Med. 18 (10) (2014) 2082–2091.
[32] U. Grohmann, C. Volpi, F. Fallarino, S. Bozza, R. Bianchi, C. Vacca, C. Orabona, M.L. Belladonna, E. Ayroldi, G. Nocentini, L. Boon, F. Bistoni, M.C. Fioretti, L. Romani, C. Riccardi, P. Puccetti, Reverse signaling through GITR ligand enables dexamethasone to activate IDO in allergy, Nat. Med. 13 (5) (2007) 579–586.
[33] M.T. Nelp, P.A. Kates, J.T. Hunt, J.A. Newitt, A. Balog, D. Maley, X. Zhu, L. Abell, A. Allentoff, R. Borzilleri, H.A. Lewis, Z. Lin, S.P. Seitz, C. Yan, J.T. Groves, Immune-modulating enzyme indoleamine 2,3-dioxygenase is effectively inhibited by targeting its apo-form, Proc. Natl. Acad. Sci. U.S.A. 115 (13) (2018) 3249–3254.
[34] U.F. Rohrig, S.R. Majjigapu, A. Grosdidier, S. Bron, V. Stroobant, L. Pilotte, D. Colau, P. Vogel, B.J. Van den Eynde, V. Zoete, O. Michielin, Rational design of 4-aryl-1,2,3-triazoles for indoleamine 2,3-dioxygenase 1 inhibition, J. Med. Chem. 55 (11) (2012) 5270–5290.
[35] U.F. Rohrig, S.R. Majjigapu, M. Chambon, S. Bron, L. Pilotte, D. Colau, B.J. Van den Eynde, G. Turcatti, P. Vogel, V. Zoete, O. Michielin, Detailed analysis and follow-up studies of a high-throughput screening for indoleamine 2,3-dioxygenase 1 (IDO1) inhibitors, Eur. J. Med. Chem. 84 (2014) 284–301.
[36] A. Habara-Ohkubo, O. Takikawa, R. Yoshida, Cloning and expression of a cDNA encoding mouse indoleamine 2,3-dioxygenase, Gene 105 (2) (1991) 221–227.
[37] O. Takikawa, T. Kuroiwa, F. Yamazaki, R. Kido, Mechanism of interferon-gamma action. Characterization of indoleamine 2,3-dioxygenase in cultured human cells induced by interferon-gamma and evaluation of the enzyme-mediated tryptophan degradation in its anticellular activity, J. Biol. Chem. 263 (4) (1988) 2041–2048.
[38] G. Mondanelli, R. Bianchi, M.T. Pallotta, C. Orabona, E. Albini, A. Iacono, M.L. Belladonna, C. Vacca, F. Fallarino, A. Macchiarulo, S. Ugel, V. Bronte, F. Gevi, L. Zolla, A. Verhaar, M. Peppelenbosch, E.M. Mazza, S. Bicciato, Y. Laouar, L. Santambrogio, P. Puccetti, C. Volpi, U. Grohmann, A relay pathway between arginine and tryptophan metabolism confers immunosuppressive properties on dendritic cells, Immunity 46 (2) (2017) 233–244.
[39] A. Bessede, M. Gargaro, M.T. Pallotta, D. Matino, G. Servillo, C. Brunacci, S. Bicciato, E.M. Mazza, A. Macchiarulo, C. Vacca, R. Iannitti, L. Tissi, C. Volpi, M.L. Belladonna, C. Orabona, R. Bianchi, T.V. Lanz, M. Platten, M.A. Della Fazia, D. Piobbico, T. Zelante, H. Funakoshi, T. Nakamura, D. Gilot, M.S. Denison, G.J. Guillemin, J.B. DuHadaway, G.C. Prendergast, R. Metz, M. Geffard, L. Boon, M. Pirro, A. Iorio, B. Veyret, L. Romani, U. Grohmann, F. Fallarino, P. Puccetti, Aryl hydrocarbon receptor control of a disease tolerance defence pathway, Nature 511 (7508) (2014) 184–190.
[40] C. Volpi, F. Fallarino, M.T. Pallotta, R. Bianchi, C. Vacca, M.L. Belladonna, C. Orabona, A. De Luca, L. Boon, L. Romani, U. Grohmann, P. Puccetti, High doses of CpG oligodeoxynucleotides stimulate a tolerogenic TLR9-TRIF pathway, Nat. Commun. 4 (2013) 1852.
[41] C. Orabona, P. Puccetti, C. Vacca, S. Bicciato, A. Luchini, F. Fallarino, R. Bianchi, E. Velardi, K. Perruccio, A. Velardi, V. Bronte, M.C. Fioretti, U. Grohmann, Toward the identification of a tolerogenic signature in IDO-competent dendritic cells, Blood 107 (7) (2006) 2846–2854.
[42] C. Orabona, E. Tomasello, F. Fallarino, R. Bianchi, C. Volpi, S. Bellocchio, L. Romani, M.C. Fioretti, E. Vivier, P. Puccetti, U. Grohmann, Enhanced tryptophan catabolism in the absence of the molecular adapter DAP12, Eur. J. Immunol. 35 (11) (2005) 3111–3118.
[43] P. Puccetti, R. Bianchi, M.C. Fioretti, E. Ayroldi, C. Uyttenhove, A. Van Pel, T. Boon, U. Grohmann, Use of a skin test assay to determine tumor-specific CD8+ T cell reactivity, Eur. J. Immunol. 24 (6) (1994) 1446–1452.
[44] M. Irla, N. Kupfer, T. Suter, R. Lissilaa, M. Benkhoucha, J. Skupsky, P.H. Lalive, A. Fontana, W. Reith, S. Hugues, MHC class II-restricted antigen presentation by plasmacytoid dendritic cells inhibits T cell-mediated autoimmunity, J. Exp. Med. 207 (9) (2010) 1891–1905.
[45] W. Chen, IDO: more than an enzyme, Nat. Immunol. 12 (9) (2011) 809–811.
[46] C. Uyttenhove, L. Pilotte, I. Theate, V. Stroobant, D. Colau, N. Parmentier, T. Boon, B.J. Van den Eynde, Evidence for a tumoral immune resistance mechanism based on tryptophan degradation by indoleamine 2,3-dioxygenase, Nat. Med. 9 (10) (2003) 1269–1274.
[47] C. Orabona, G. Mondanelli, P. Puccetti, U. Grohmann, Immune checkpoint molecules, personalized immunotherapy, and autoimmune diabetes, Trends Mol. Med. (2018).
[48] U.F. Rohrig, S.R. Majjigapu, P. Vogel, V. Zoete, O. Michielin, Challenges in the discovery of indoleamine 2,3-dioxygenase 1 (IDO1) inhibitors, J. Med. Chem. 58 (24) (2015) 9421–9437.
[49] G.C. Prendergast, A. Mondal, S. Dey, L.D. Laury-Kleintop, A.J. Muller, Inflammatory reprogramming with IDO1 inhibitors: turning immunologically unresponsive 'cold' tumors 'hot', Trends Cancer 4 (1) (2018) 38–58.
[50] A. Mullard, IDO takes a blow, Nat. Rev. Drug Discovery 17 (5) (2018) 307.
[51] K. Garber, A new cancer immunotherapy suffers a setback, Science (New York, N.Y.) 360 (6389) (2018) 588.
[52] Y. Liu, X. Liang, W. Dong, Y. Fang, J. Lv, T. Zhang, R. Fiskesund, J. Xie, J. Liu, X. Yin, X. Jin, D. Chen, K. Tang, J. Ma, H. Zhang, J. Yu, J. Yan, H. Liang, S. Mo, F. Cheng, Y. Zhou, H. Zhang, J. Wang, J. Li, Y. Chen, B. Cui, Z.W. Hu, X. Cao, F. Xiao-Feng Qin, B. Huang, Tumor-Repopulating Cells Induce PD-1 Expression in CD8(+) T Cells by Transferring Kynurenine and AhR Activation, Cancer Cell 33 (3) (2018) 480–494.e7.
[53] B.J. Moyer, I.Y. Rojas, I.A. Murray, S. Lee, H.F. Hazlett, G.H. Perdew, C.R. Tomlinson, Indoleamine 2,3-dioxygenase 1 (IDO1) inhibitors activate the aryl hydrocarbon receptor, Toxicol. Appl. Pharmacol. 323 (2017) 74–80.
[54] F. Anquetil, G. Mondanelli, N. Gonzalez, T. Rodriguez Calvo, J. Zapardiel Gonzalo, L. Krogvold, K. Dahl-Jorgensen, B. Van den Eynde, C. Orabona, Loss of IDO1 expression from human pancreatic beta-cells precedes their destruction during the development of type 1 diabetes, Diabetes 67 (9) (2018) 1858–1866.
[55] C. Orabona, G. Mondanelli, M.T. Pallotta, A. Carvalho, E. Albini, F. Fallarino, C. Vacca, C. Volpi, M.L. Belladonna, M.G. Berioli, G. Ceccarini, S.M. Esposito, R. Scattoni, A. Verrotti, A. Ferretti, G. De Giorgi, S. Toni, M. Cappa, M.C. Matteoli, R. Bianchi, D. Matino, A. Iacono, M. Puccetti, C. Cunha, S. Bicciato, C. Antognelli, V.N. Talesa, L. Chatenoud, D. Fuchs, L. Pilotte, B. Van den Eynde, M.C. Lemos, L. Romani, P. Puccetti, U. Grohmann, Deficiency of immunoregulatory indoleamine 2,3-dioxygenase 1in juvenile diabetes, JCI Insight 3 (6) (2018).